

# Analytical and numerical study of the apparent diffusion coefficient in diffusion MRI at long diffusion times and low b-values

Jing-Rebecca Li, Denis Le Bihan, Thong Quoc Nguyen, Denis Grebenkov, Cyril Poupon, Housseem Haddar

► **To cite this version:**

Jing-Rebecca Li, Denis Le Bihan, Thong Quoc Nguyen, Denis Grebenkov, Cyril Poupon, et al.. Analytical and numerical study of the apparent diffusion coefficient in diffusion MRI at long diffusion times and low b-values. 2012. hal-00763885

**HAL Id: hal-00763885**

**<https://hal.inria.fr/hal-00763885>**

Preprint submitted on 14 Dec 2012

**HAL** is a multi-disciplinary open access archive for the deposit and dissemination of scientific research documents, whether they are published or not. The documents may come from teaching and research institutions in France or abroad, or from public or private research centers.

L'archive ouverte pluridisciplinaire **HAL**, est destinée au dépôt et à la diffusion de documents scientifiques de niveau recherche, publiés ou non, émanant des établissements d'enseignement et de recherche français ou étrangers, des laboratoires publics ou privés.

# Analytical and numerical study of the apparent diffusion coefficient in diffusion MRI at long diffusion times and low b-values

J.R. Li<sup>1,2\*</sup>, D. Le Bihan<sup>2</sup>, T.Q. Nguyen<sup>1</sup>, D. Grebenkov<sup>3</sup>, C. Poupon<sup>2</sup>, H. Haddar<sup>1</sup>

<sup>1</sup>INRIA Saclay Equipe DEFI, CMAP Ecole Polytechnique, Palaiseau Cedex, France

<sup>2</sup>NeuroSpin, CEA-Saclay Center Gif sur Yvette, France

<sup>3</sup>LPMC CNRS Ecole Polytechnique, Palaiseau, France

**Running title: ADC at long diffusion times and low b values**

## **Correspondent:**

Jing-Rebecca Li

INRIA Saclay-Equipe DEFICMAP, Ecole Polytechnique

Route de Saclay, 91128, Palaiseau Cedex, France

jingrebecca.li@inria.fr

+33-1-69-08-94-82

**Word count: 4096**

## **Abstract**

Diffusion magnetic resonance imaging provides a measure of the average distance travelled by water molecules in a medium and can give useful information on cellular structure and structural change when the medium is biological tissue. In this paper, two approximate models for the apparent diffusion coefficient at low b-values and long diffusion times are formulated and validated. The first is a steady-state partial differential equation model that gives the steady-state (infinite time) effective diffusion tensor for general cellular geometries. For nearly isotropic diffusion where the intracellular compartment consists of non-elongated cells, a second approximate model is provided in the form of analytical formulae for the eigenvalue of the steady-state effective diffusion tensor. Both models are validated by numerical simulations on a variety of cells sizes and shapes.

**Keywords:** Diffusion MRI, Simulation, Bloch-Torrey, ADC

# Introduction

Diffusion MRI (DMRI) provides a measure of the average distance travelled by water molecules in tissues and can give useful information on tissue structure and changes that occur when the tissue is challenged physiologically or pathologically. A large number of works have appeared in the last 25 years that show that DMRI measurements can be correlated with various physiological or pathological conditions, especially, but not only, in the brain [1]. The most striking example comes from the detection of acute cerebral ischemia on the basis of lower than normal apparent diffusion coefficient a few minutes after stroke [2, 3]. Diffusion MRI also has been used for cancer detection and treatment monitoring, as diffusion seems to be linked to tumor cellularity [4, 5, 6]. Finally, recent work has suggested that water diffusion MRI could also be used to visualize changes in tissue microstructure that might arise during neuronal activation: a transient decrease in water diffusion has been reported in the human brain visual cortex during activation by a black and white flickering checkerboard [7]. Based on the known sensitivity of diffusion MRI to cell size in tissues [8, 9] and on optical imaging studies that have revealed changes in the shape (in particular swelling) of neurons and glial cells during brain activation [10, 11, 12], the observed ADC findings have been tentatively ascribed to a transient swelling of cortical cells.

However, even though the potential applications of diffusion MRI have multiplied rapidly, the understanding of the exact biophysical mechanisms behind the properties of water diffusion measurements obtained by MRI in biological tissue is still limited. In most articles that demonstrate a statistically significant correlation between the measured DMRI signal and some physiological or pathological parameters, the connection is usually explained only qualitatively.

The effort to make a more quantitative connection between tissue properties and the measured diffusivity has led to the development of various biophysical models. Solutions to such models can be obtained analytically in some simple conditions, for instance, assuming infinitely short duration gradient pulses and a diffusion partial

differential equation (PDE) model in simple geometries [13, 14]). For more realistic modeling, validation can be obtained using computer simulations on PDE models [15, 16, 17] or using Monte-Carlo simulations of the individual diffusive displacements of water molecules in given tissue configurations [18, 19]. Whenever possible, validation must be obtained *in vivo* using biological models where certain tissue parameters have been controlled. *In vivo* experiments can also be used to estimate some parameters required by the biophysical models [20].

In this article, we consider the diffusion MRI signal attenuation at relatively long diffusion times and low b-values. We start with the multiple compartments Bloch-Torrey PDE [21, 22] as the full, ‘gold-standard’, model. We show that the apparent diffusion coefficient, which depends on the diffusion gradient direction vector  $\mathbf{q}/\|\mathbf{q}\|$ , of the DMRI signal obtained at low b-values, or more precisely, the slope of the log signal versus b-value curve at b=0, which we denote by  $ADC_0(\mathbf{q}/\|\mathbf{q}\|)$ , converge to a limit as the diffusion time increases. We call this limit the steady-state limit of the  $ADC_0$ . We show that, for general cellular geometries, this steady-state limit can be obtained by solving a set of time-independent PDEs using mathematical homogenization theory [23] to obtain the homogenized diffusion tensor which we denote by  $\mathbf{D}^H$ . In other words,  $ADC_0(\mathbf{q}/\|\mathbf{q}\|)$  approaches  $\mathbf{q}^T \mathbf{D}^H \mathbf{q} / \|\mathbf{q}\|^2$ , as the diffusion time increases to infinity. In addition, we show that if the diffusion is nearly isotropic, i.e., if for any  $\mathbf{q}$ ,  $\mathbf{q}^T \mathbf{D}^H \mathbf{q} / \|\mathbf{q}\|^2 = D^H$  (a homogenized diffusion coefficient) and if the intra-cellular compartment is made up of cells that are not elongated,  $D^H$  can be accurately approximated by two existing analytical models that relate  $D^H$  to the biophysical parameters of the tissue, namely, the diffusion coefficients in compartments, the membrane permeability and the average inter-cell distance.

Our numerical analysis uses experimental parameters typically obtained with clinical scanners, i.e., using pulsed gradient spin-echo (PGSE) sequences with somewhat long diffusion times (e.g. 10-85 ms) and low b-values (b between 0 and 500 s/mm<sup>2</sup>). First, we will show that a three-compartment model of tissue, consisting of the intra-cellular, the extra-cellular, and membrane compartments, can be replaced by a two-compartment model consisting of only the intra-cellular and extra-cellular

compartments, along with a permeability condition on the infinitely thin interface between the intra and extra-cellular compartments. Next, we will show that  $ADC_o(\mathbf{q}/\|\mathbf{q}\|)$  approaches  $\mathbf{q}^T \mathbf{D}^H \mathbf{q} / \|\mathbf{q}\|^2$  as the diffusion time increases for general two-compartment tissue geometries, including a configuration of many randomly oriented and placed cylindrical and spherical cells. Finally, given the additional assumption that the cells are not too elongated and that the diffusion is nearly isotropic, we show that two existing analytical models give good approximations to the homogenized diffusion coefficient,  $D^H = \mathbf{q}^T \mathbf{D}^H \mathbf{q} / \|\mathbf{q}\|^2$  for any  $\mathbf{q}$ . We support this last conclusion by numerical simulations on periodic arrays of cubic cells, spherical cells squeezed to high volume fraction, and polyhedral cells. We then analyze how  $D^H$  is sensitive to tissue parameters and show that at low permeability,  $D^H$  is mainly influenced by the extracellular space.

## Theory

### ***Multiple-compartment Bloch Torrey PDE model with finite permeability***

The water magnetization in biological tissue in the presence of applied magnetic field gradient pulses at the voxel level can be modeled by a multiple compartment Bloch-Torrey PDE [21, 22] and this model is our starting point. This model is complex enough to incorporate some interesting and useful biological properties of tissue, but at the same time, it is sufficiently simple to allow theoretical analysis. In this article we consider the tissue to be made of two compartments,  $\Omega^i$  and  $\Omega^e$ , representing the ensemble of homogeneous intracellular spaces, and the extra-cellular space, respectively. We model the cell membranes as infinitely thin (compared to cell size) permeable interfaces. However, we will also show that a three-compartment model, where the third compartment is the membrane layer, approaches the diffusion behavior of the two-compartment model as the thickness of the membrane layer goes to 0 if we replace the membrane layer by an infinitely thin interface with permeability  $\kappa = D^m/h$ , where  $D^m$  is the diffusion coefficient inside the membrane and  $h$  is the membrane

thickness. Thus, any results we obtain for the two-compartment model can be applied directly to the three-compartment model if the membrane layer is thin.

The two/three compartment Bloch-Torrey PDE model should be seen as a starting point to investigate the relationship of cellular geometry to measured diffusivity. More complex models may also be introduced, for instance considering a compartment of water molecules in interaction with membranes [11], but this is out of the scope of this work.

We start from a mass of water molecules located at  $\mathbf{x}_0$  at  $t = 0$  and we search for the magnetization at time  $t$  due this initial density. For a given magnetic field gradient with normalized time profile  $g(t)$ ,  $\max(\text{abs}(g(t)))=1$ , intensity  $\|\mathbf{G}\|$  and direction vector  $\mathbf{G}/\|\mathbf{G}\|$ , the magnetization in compartment  $\Omega^j$  (where  $j$  can be  $i$ ,  $e$ , the intra-cellular or the extra-cellular compartment, respectively), denoted  $m^j$ , satisfies the Bloch-Torrey PDE:

$$\frac{\partial m^j(\mathbf{x}, t, |\mathbf{x}_0, \mathbf{q})}{\partial t} = i g(t)(\mathbf{q} \cdot \mathbf{x})m^j(\mathbf{x}, t, |\mathbf{x}_0, \mathbf{q}) + \nabla \cdot (D^j \nabla m^j(\mathbf{x}, t, |\mathbf{x}_0, \mathbf{q})), \mathbf{x} \in \Omega^j . \quad [1]$$

with  $\mathbf{q} := \gamma \mathbf{G}$ , where  $\gamma$  is the gyromagnetic ratio of water proton. We note here that  $g(t)$  is made negative for  $t \geq TE/2$ , where  $TE$  is the echo time. The intrinsic diffusion coefficients in the intra-cellular and extra-cellular compartments are  $D^i$ ,  $D^e$ , respectively.

The initial mass can be located anywhere in the voxel:

$$m^j(\mathbf{x}, 0, |\mathbf{x}_0, \mathbf{q}) = \delta(\mathbf{x} - \mathbf{x}_0), \quad \mathbf{x}_0 \in \Omega^i \cup \Omega^e. \quad [2]$$

The PDE in Eq. [1] and the initial condition in Eq. [2] need to be supplemented by interface conditions where two compartments come together. The first is the conservation of flux:

$$D^j \nabla m^j(\mathbf{x}, t, |\mathbf{x}_0, \mathbf{q}) \cdot \mathbf{n}^j(\mathbf{x}) = -D^k \nabla m^k(\mathbf{x}, t, |\mathbf{x}_0, \mathbf{q}) \cdot \mathbf{n}^k(\mathbf{x}), \quad \mathbf{x} \in \Gamma^{jk}, \quad [3]$$

where  $\mathbf{n}^k$  is the outward pointing normal and  $\Gamma^{jk}$  is the interface between compartments  $j$  and  $k$ , and the second is a permeability condition:

$$D^j \nabla m^j(\mathbf{x}, t, |\mathbf{x}_0, \mathbf{q}) \cdot \mathbf{n}^j(\mathbf{x}) = \kappa (m^j(\mathbf{x}, t, |\mathbf{x}_0, \mathbf{q}) - m^k(\mathbf{x}, t, |\mathbf{x}_0, \mathbf{q})), \quad \mathbf{x} \in \Gamma^{jk}, \quad [4]$$

where  $\kappa$  is the membrane permeability. The total signal (non-normalized) is then

$$\Psi(\mathbf{q}, t) = \int_{\mathbf{x}_0 \in \Omega^i \cup \Omega^e} d\mathbf{x}_0 \sum_{j=i,e} \int_{\mathbf{x} \in \Omega^j} m^j(\mathbf{x}, t, |\mathbf{x}_0, \mathbf{q}) d\mathbf{x} , \quad [5]$$

where the integral is taken over all compartments and all initial conditions.

In a homogeneous medium with free (hence Gaussian) diffusion, the plot of the log of the signal versus  $b$ -value, where the  $b$ -value depends on  $\mathbf{q}$  and  $t$  as:

$$b(\mathbf{q}, t) = \|\mathbf{q}\|^2 \int_0^t du \left( \int_0^u g(s) ds \right)^2, \quad [6]$$

would be linear and the slope of the line, also called the first moment with respect to  $b$ -value, would be the intrinsic diffusion coefficient. In biological tissue, the medium is heterogeneous. Fitting the data by a straight line thus leads only to an “apparent diffusion coefficient” (ADC) which is a complex mixture of the tissue parameters [24]:

$$\min_{\{ADC\}} \sum_j \left\| \log \frac{\Psi(b_j)}{\Psi(0)} - (-ADC * b_j) \right\|^2. \quad [7]$$

However, at high  $b$  values (above 1000s/mm<sup>2</sup> in the brain) the log of the signal attenuation is not linear with the  $b$ -value because diffusion is not Gaussian [25] at physically relevant diffusion times. Because of the curvature of log signal curve, the ADC appears to depend on the  $b$ -value and a more comprehensive model must be used. For instance, the log signal curve can be fitted by a bi-exponential [26, 11]:

$$\min_{\{v^f, D^f, D^s\}} \sum_j \left\| \frac{\Psi(b_j)}{\Psi(0)} - \left( v^f e^{-D^f b_j} + (1 - v^f) e^{-D^s b_j} \right) \right\|^2, \quad [8]$$

where  $D^f$  and  $D^s$ ,  $v^f$ ,  $1-v^f$ , are the fitted diffusion coefficients and volume fractions of two Gaussian diffusion pools. In the limit of short diffusion time,  $D^f$  and  $D^s$ ,  $v^f$ ,  $1-v^f$ , have physical interpretation as the intrinsic diffusion coefficients of the two pools, for instance the extra-cellular and intra-cellular compartments and their respective volume fractions. However, when the diffusion time increases, because of the exchange between the pools those fitted parameters become complicated mixture of the intrinsic diffusion coefficients, the exchange time (or the permeability) between the compartments, their shapes, and the acquisition parameters [27].

The log signal curve can also be fitted as a cumulant expansion of the  $b$ -value. Limiting to the second order (quadratic polynomial) in  $b$ -value one gets [28, 29]:

$$\min_{\{ADC_0, KUR_0\}} \sum_j \left\| \log \frac{\Psi(b_j)}{\Psi(0)} - \left( -ADC_0 b_j + \frac{1}{6} KUR_0 ADC_0^2 b_j^2 \right) \right\|^2, \quad [9]$$



where  $KUR_0$  is called Kurtosis and characterizes the deviation of the signal from a mono-exponential decay in  $b$ -value. In this article we denoted the linear term (the first moment with respect to  $b$ -value) by  $ADC_0$  instead of ADC (as a deviation from the notation in [28, 29]) to distinguish it from the ADC defined by Eq. [7].  $ADC_0$  can be thought of as the derivative of the fitted quadratic polynomial function, extrapolated to  $b = 0$ . If we take the derivative of the the bi-exponential function in Eq. [8] at  $b = 0$ , we obtain:

$$ADC_0 = v^f D^f + (1 - v^f) D^s \quad [10]$$

thus, making a connection between the bi-exponential model and  $ADC_0$ .

It is important to note that although  $ADC_0$  is independent of the  $b$ -value by construction, it is no longer an intrinsic parameter and highly depends on the diffusion time, as well as the combined tissue properties, the object of this work.

### ***Effective diffusion tensor of homogenization***

In a homogeneous medium, the  $ADC_0$  would be simply the intrinsic diffusion coefficient. At long diffusion times, water molecules have had time to travel a diffusion distance that is long compared to the average size of the cells (hence water molecules switch back and forth between the intra and extracellular compartments several times), one can expect that some kind of ‘effective’ diffusion tensor can be used to describe the average diffusion behavior.

We have used the theory of homogenization to obtain the infinite diffusion time effective diffusion tensor  $\mathbf{D}^H$ . Because homogenized equations are usually formulated for problems with infinite permeability,  $\kappa = \infty$ , on the interface between different compartments, we had to make a limit argument on the width of the interface to obtain the set of steady-state PDE below (see derivation in the Appendix) taking into account a finite permeability  $\kappa < \infty$  between the intra-cellular and extra-cellular compartments. At the same time, this limit argument can also be used to justify the replacement of the

three-compartment model comprising of the intra-cellular, the extra-cellular, and a thin membrane layer compartment (with  $\kappa = \infty$ ) by a two-compartment model where the membrane layer is replaced by an infinitely thin interface with permeability  $\kappa = D^m/h$ , where  $D^m$  is the intrinsic diffusion coefficient in the membrane layer, and  $h$  is the membrane layer thickness. Similar equations have first appeared in [30] in the context of effective conductivity, but as far as we know, these equations have not been used in the modeling the long time diffusion MRI signals in the presence of finitely permeable membranes.

In mathematical homogenization theory [23] a series solution of the diffusion problem can be formulated in powers of  $\varepsilon$ , where  $\varepsilon$  is the length scale of the spatial variation of the medium, in our case, around the average cell size. The leading order solution, which we will describe below, is accurate when  $\varepsilon$  is small compared to the diffusion distance.

We assume the computational domain is a cube, denoted  $\mathbf{C}$ , with side length  $W$ :  $\mathbf{C} = [0, W] \times [0, W] \times [0, W]$ , that contains a configuration of cells. The computational cube  $\mathbf{C}$  is assumed to repeat periodically in all three coordinate directions many times to make up one voxel. We assume  $\mathbf{C}$  is small compared to the size of the voxel from which we get the DMRI signal. Hence, we can make the approximation that  $\mathbf{C}$  is repeated an infinite number of times in all three coordinate directions.

The homogenized diffusion tensor  $\mathbf{D}^H$  is given by

$$\mathbf{D}^H = \begin{pmatrix} D_{11}^H & D_{12}^H & D_{13}^H \\ D_{21}^H & D_{22}^H & D_{23}^H \\ D_{31}^H & D_{32}^H & D_{33}^H \end{pmatrix} \quad [11]$$

where the entries of the matrix are:

$$D_{mp}^H = \frac{1}{\text{vol}(\mathbf{C})} \sum_{j=i,e} \int_{\Omega^j} D^j \nabla u_m^j(\mathbf{x}) \cdot \mathbf{e}_p \, d\mathbf{x} \quad , \quad [12]$$

and where the auxiliary function  $u_m(\mathbf{x})$  is defined piecewise on  $\Omega^j$  and satisfies the time-independent PDE

$$\begin{aligned}
\nabla \cdot (D^j \nabla u_m^j(\mathbf{x})) &= 0, & \mathbf{x} \in \Omega^j, & & j = i, e, \\
D^j \nabla u_m^j(\mathbf{x}) \cdot \mathbf{n}^j(\mathbf{x}) &= -D^k \nabla u_m^k(\mathbf{x}) \cdot \mathbf{n}^k(\mathbf{x}), & x \in \Gamma^{jk}, & & j, k = i, e, \\
D^j \nabla u_m^j(\mathbf{x}) \cdot \mathbf{n}^j(\mathbf{x}) &= \kappa (u_m^j(\mathbf{x}) - u_m^k(\mathbf{x})), & \mathbf{x} \in \Gamma^{jk}, & & \\
u_m(\mathbf{x} + W \mathbf{e}_m) &= u_m(\mathbf{x}) + W, & x, x + W \mathbf{e}_m \in \partial \mathbf{C}, & & \\
u_m(\mathbf{x} + W \mathbf{e}_n) &= u_m(\mathbf{x}), & x, x + W \mathbf{e}_n \in \partial \mathbf{C}, n \neq m. & &
\end{aligned} \tag{13}$$

The vector  $\mathbf{e}_m$  is the unit vector in the  $m^{\text{th}}$  coordinate direction. In summary, to obtain  $\mathbf{D}^H$  we solve three time-independent equations of the form in Eq. [13] for each of the three coordinate directions and use the formula in Eq. [12]. We note that the PDE in Eq. [13] does not depend on time and the diffusion gradient, hence it is less computationally expensive to solve than the original time-dependent Bloch-Torrey equation. At long diffusion times,  $\text{ADC}_0$ , computed by solving the Bloch-Torrey PDE numerically, should approach the steady-state value,  $\frac{\mathbf{q}^T \mathbf{D}^H \mathbf{q}}{\|\mathbf{q}\|^2}$ , predicted by the homogenized diffusion tensor (see [23]).

### ***Analytical approximations for the isotropic two-compartment effective diffusion tensor***

In a nearly isotropic medium, the eigenvalues of  $\mathbf{D}^H$  are approximately equal. The effective diffusion tensor  $\mathbf{D}^H$  can then be replaced by an effective diffusion coefficient  $D^H$ . In the case of two compartments, the intra-cellular and the extra-cellular spaces, there are approximate analytical expressions for  $D^H$  in the literature for periodically placed spherical cells.

In the field of composite media the following analytical approximations for  $D^H$  were given for circular cells in two dimensions (denoted here  $D_{HJ}$  for Hasselman and Johnson) [31] and spherical cells in three dimensions (denoted here  $D_{TR}$  for Torquato and Rintoul) [32]:

$$\begin{aligned}
D_{HJ} &= D^e \left( \frac{\left( \frac{D^i}{D^e} - \frac{D^i}{R\kappa} - 1 \right) v^i + \frac{D^i}{D^e} + \frac{D^i}{R\kappa} + 1}{\left( 1 - \frac{D^i}{D^e} + \frac{D^i}{R\kappa} \right) v^i + \frac{D^i}{D^e} + \frac{D^i}{R\kappa} + 1} \right), \quad d = 2, \\
D_{TR} &= D^e \left( \frac{2 \left( \frac{D^i}{D^e} - \frac{D^i}{R\kappa} - 1 \right) v^i + \frac{D^i}{D^e} + \frac{2D^i}{R\kappa} + 2}{\left( 1 - \frac{D^i}{D^e} + \frac{D^i}{R\kappa} \right) v^i + \frac{D^i}{D^e} + \frac{2D^i}{R\kappa} + 2} \right), \quad d = 3,
\end{aligned} \tag{14}$$

$d$  being the space dimension (2 or 3),  $R$  the radius of the cells,  $\kappa$  is the membrane permeability,  $v^i$  is the intra-cellular volume fraction, and  $v^e = 1 - v^i$  is the extra-cellular volume fraction. To generalize this formula to non-spherical cells, we replace  $R$  with the following expression

$$R = L \left( c \frac{v^i}{\pi} \right)^{\frac{1}{d}}, \quad c = 1 \text{ if } d = 2, \quad c = \frac{3}{4} \text{ if } d = 3, \tag{15}$$

where  $L$  is the distance between the nearest cell centers. We prefer to use  $L$  (called the average inter-cell distance in the rest of the paper) instead of  $R$  because the formula will be applied to geometries containing multiple cells of different shapes and sizes. In that case, an average radius may be not well defined, whereas an average inter-cell distance is easily defined: we simply count how many cells are in the computational domain  $\mathbf{C}$  and define  $L$  by

$$L \equiv \frac{W}{n_{cell}^{\frac{1}{3}}}, \tag{16}$$

where  $W$  is the side length of  $\mathbf{C}$ . In other words,  $L$  is the inverse of the cubic root the cellularity (number of cells per unit volume).

An early paper in the field of diffusion MRI contains a different analytical approximation. In [33] the following formula was proposed to approximate  $D^H$  in the case of spherical cells (not valid for 2 dimensional disks):

$$\frac{D_{LSMS} - u}{D^e - u} \left( \frac{D^e}{D_{LSMS}} \right)^{\frac{1}{d}} = 1 - v^i, \quad u \equiv \frac{\kappa R D^i}{\kappa R + D^i}, \tag{17}$$

where we denote the  $D^H$  approximation by  $D_{LSMS}$  for the four authors Latour, Svoboda, Mitra, Sotak. We also will replace  $R$  with the expression in Eq. [15].

Finally, we mention one more analytical formula for  $D^H$ , denoted  $D_{NFJH}$  for the authors, in the special case when the extra-cellular volume fraction is 0, i.e., when  $v^j = 1$ , given in [34]:

$$D_{NFJH} = \frac{D^i}{1 + \xi}, \quad \xi \equiv \frac{D^i}{\kappa L}, \quad [18]$$

which is valid for two and three dimensions.

The approximations for  $D^H$ ,  $D_{HJ}$  (2D),  $D_{TR}$ (3D),  $D_{LSPS}$ (3D), and  $D_{NFJH}$  (2D and 3D), are called analytical approximations because they are given by simple explicit formulae. These analytical approximations contain five intrinsic biological parameters: the intrinsic diffusion coefficients,  $D^e$  and  $D^i$ , of the extra-cellular and intra-cellular compartments, the membrane permeability  $\kappa$ , the intra-cellular volume fraction  $v^j$ , and the average inter-cell distance  $L$ .

## Methods

We numerically solved the Bloch-Torrey PDE Eqs. [1]-[4] on the computational domain  $C = [0, W] \times [0, W] \times [0, W]$  at  $b = 0, 50, 100, 200, 500, 1000, 1500, 2000, 2500, 3000, 3500, 4000$   $s/mm^2$  for the PGSE sequence at fixed  $\delta$  and  $\Delta$  by varying the magnetic field  $\mathbf{G}$  to get a simulation of the DMRI signal decay and an estimate of  $ADC_0$ . No noise was added to the data. The pulse duration was fixed at  $\delta = 2.5ms$  and several values of  $\Delta$ , between  $10$  and  $85$   $ms$  were simulated. We imposed pseudo-periodic boundary conditions on the six faces of  $\mathbf{C}$  (same as in [16]) to mimic the effect of  $\mathbf{C}$  repeating an infinite number of times in all three coordinate directions. The numerical method we used is a finite volume space discretization coupled to Runge-Kutta Chebyshev time integration (the code was written in Matlab and Fortran90).

We estimated the time-dependent  $ADC_0$  from Eq. [9] by a quadratic fit of the calculated MRI signal in  $0 \leq b \leq 500$   $s/mm^2$ . A low range of b-values was chosen to minimize the fitting error of the slope at  $b = 0$  because in this paper we are interested foremost in how

$ADC_0$  approaches its steady-state value, rather than how  $ADC_0$  could be most robustly computed in practice. For comparison we also computed the bi-exponential fit of  $ADC_0$  from Eqs [8] and [10] in  $0 \leq b \leq 4000 \text{ s/mm}^2$  (range considered as optimal for a biexponential fit of human brain data [35]).

We computed  $\mathbf{D}^H$  by solving the steady-state PDE in Eq. [13] (the code was written in Matlab) three times, once in each coordinate direction. The computational domain is the same  $\mathbf{C}$  as for the Bloch-Torrey PDE and the spatial discretization is also the same finite volume discretization. The numerical solutions were obtained on laptop computer (DELL Latitude E6410 Intel(R) Core(TM) i7 CPU M640 @ 2,8GHz). The details of the numerical method will be the topic of a future paper.

## Results

We solved the Bloch-Torrey PDE in Eqs. [1]-[4] on four geometries shown in Fig 1A, 1B, 1C and 1D. The first (Fig 1A) is a periodic array of cubic cells with inter-cell distance  $L$ . The second (Fig 1B) is a periodic array of spherical cells with inter-cell distance  $L$  that are squeezed together: we enlarge the radius of the spheres, but we do not allow the spheres to cross each other. The squeezed spherical geometry is interesting because the cells touch their neighbors in an area that becomes larger as the cellular volume fraction increases. We can increase the cellular volume fraction of squeezed spherical cells to 100%, at which point, this geometry becomes cubic cells with no extra-cellular space. The third (Fig 1C) is a periodic array of 8 polyhedral cells with different shapes and sizes packed together, the average inter-cell distance is  $L=5 \mu\text{m}$  because there are 8 cells in a  $10^3 \mu\text{m}^3$  volume. The fourth is a combination of cylindrical cells (with diameter  $3 \mu\text{m}$ ) and spherical cells (with diameter  $8 \mu\text{m}$ ), oriented and placed randomly in a computational domain  $C = [0,175]^3 \mu\text{m}^3$  (Fig 1D is a zoom of about one tenth of the computational domain) and the extra-cellular volume fraction is  $v^e = 0.17$ , with the cylindrical cells taking 43% and the spherical cells taking 40% of the total volume fraction, respectively.

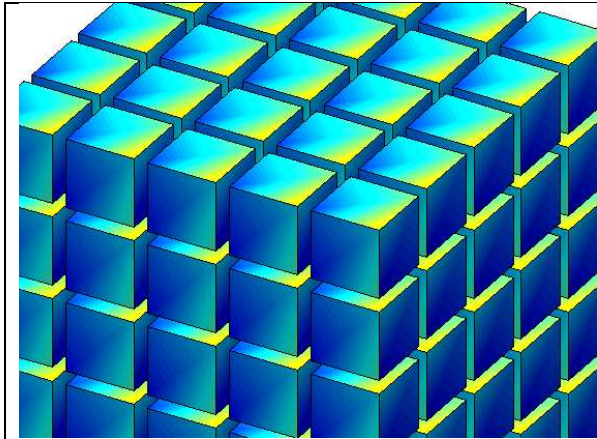


Fig 1A

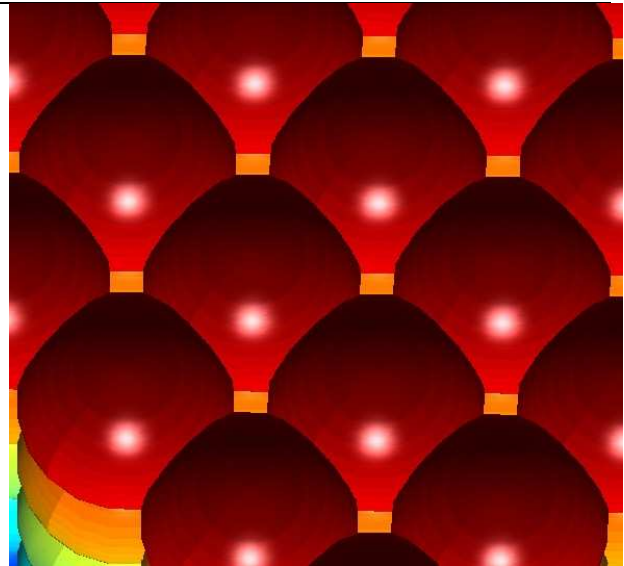


Fig 1B

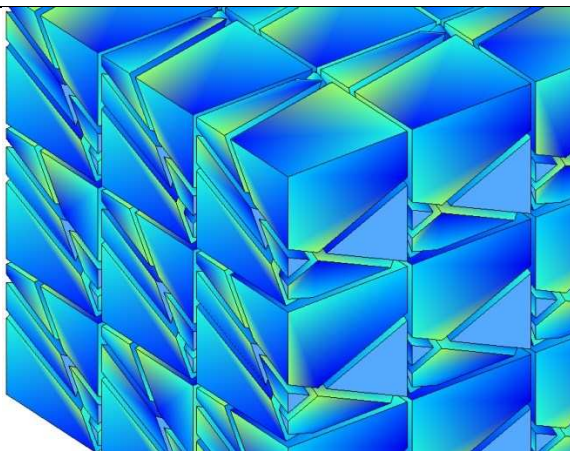


Fig 1C

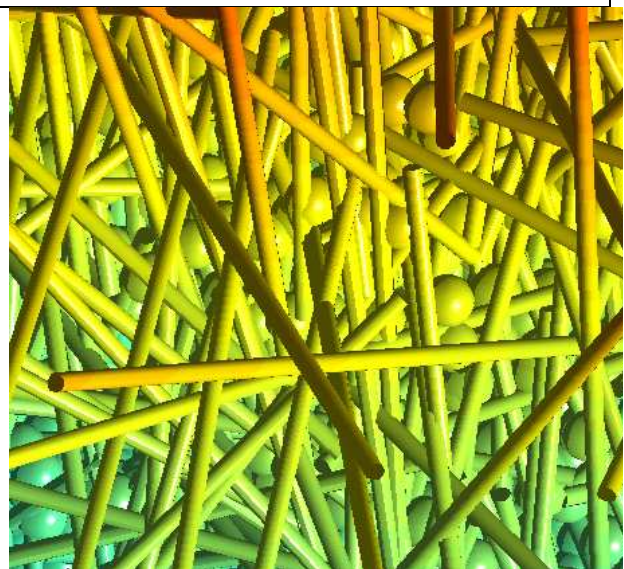


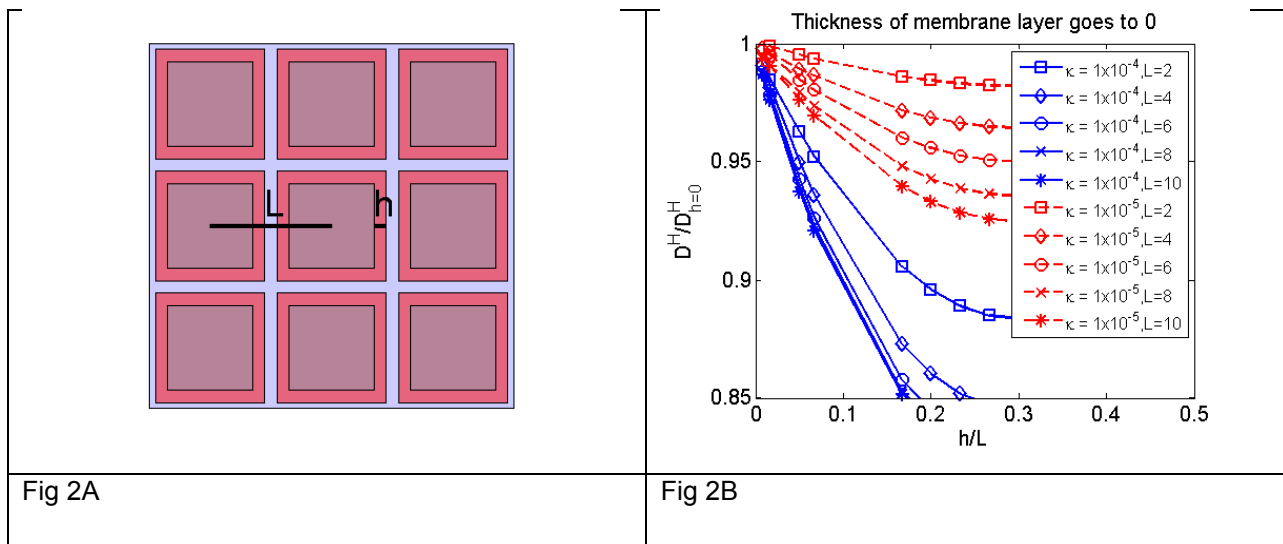
Fig 1D

### 1. *The three-compartment model*

First, we show that the homogenized diffusion tensor  $\mathbf{D}^H$  of a three-compartment model consisting of the intra-cellular, the extra-cellular, and the membrane compartments, with respective diffusion coefficients,  $D^i, D^e, D^m$ , and  $\kappa = \infty$ , can be approximated by the  $\mathbf{D}^H$  of

a two-compartment model with  $D^i$ ,  $D^e$ , and an interface condition between the intra-cellular and the extra-cellular compartments if we fix the interface permeability to be  $\kappa = D^m/h$ , where  $h$  is the thickness of the original membrane layer. The standard steady-state PDE for the three-compartment model with infinite permeability is given in Eq. [20] of the Appendix and it is a well-known result of homogenization theory [23].

We took a two-dimensional cellular geometry with periodically placed square cells with a membrane layer of thickness  $h$  and inter-cell distance  $L$  (see Fig 2A). The extra-cellular volume fraction is fixed at  $v^e = 0.13$  and  $h$  is reduced from being 30% of  $L$  to 6% of  $L$ , with  $L$  going from 2 to 10  $\mu m$ . We simulated two membrane permeabilities:  $\kappa = 10^{-4} m/s$  and  $\kappa = 10^{-5} m/s$ , in other words, setting  $D^m = \kappa h$ , for different values of  $h$ . We chose the intrinsic diffusion coefficients to be  $D^e=D^i=3 \times 10^{-3} mm^2/s$  (diffusion coefficient of free water at 37°C). We computed  $\mathbf{D}^H$  of the three-compartment model according to Eq. [20] of the Appendix and then we calculated  $\mathbf{D}^H_{h=0}$ , which is the effective tensor from the two-compartment model by solving Eq. [13]. In Fig 2B, because the diffusion is isotropic, we just plot  $D^H$ , the effective diffusion coefficient, which is the eigenvalue of  $\mathbf{D}^H$ , divided by  $D^H_{h=0}$ . We see that when  $h$  is less than 5% of  $L$ ,  $D^H$  of the three-compartment model is within 95% of  $D^H_{h=0}$  of the two-compartment model for both permeabilities.

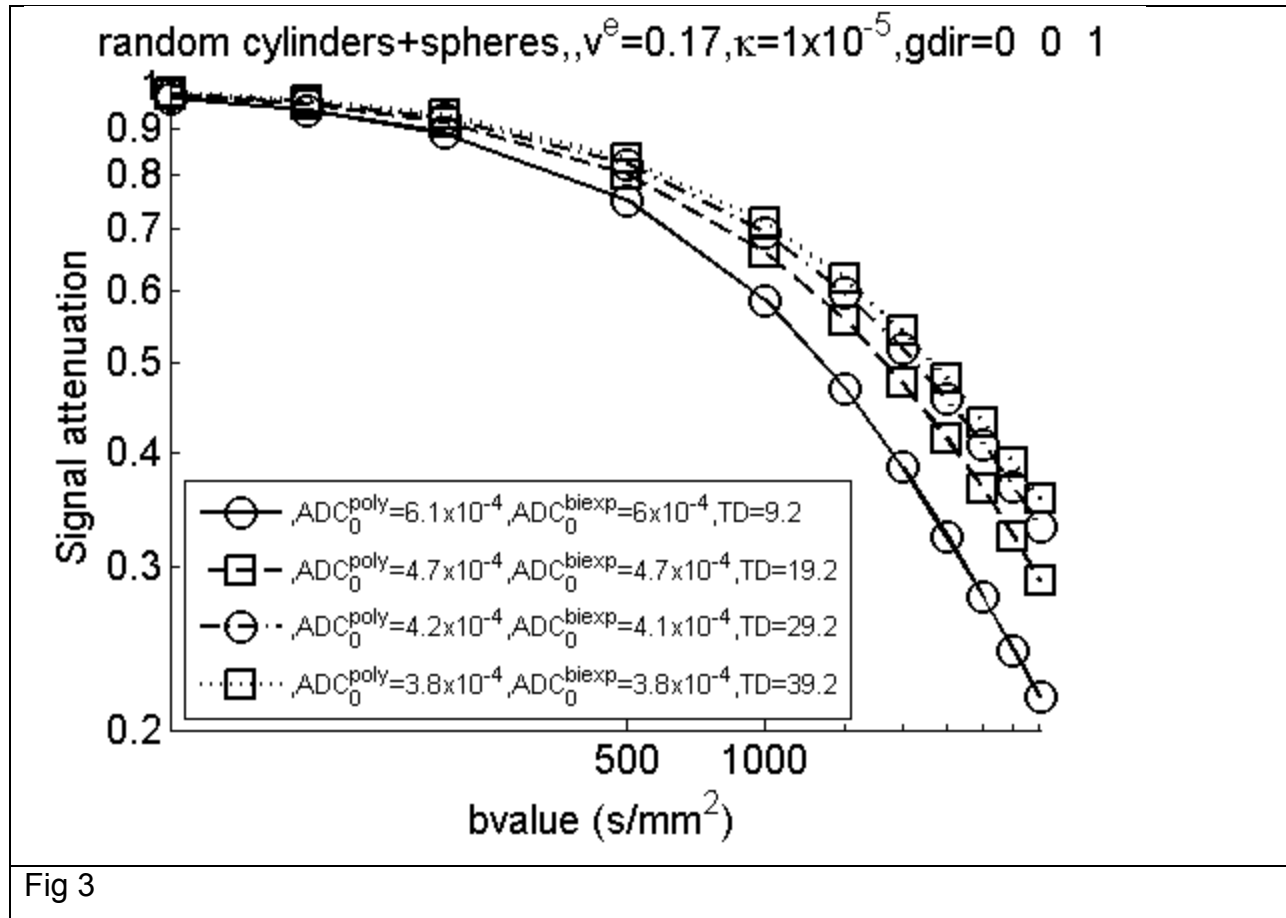




## 2. Relationship between $ADC_0$ and $D^H$

Now we show that  $ADC_0(\mathbf{q}/\|\mathbf{q}\|)$  approaches the homogenized diffusion coefficient  $\mathbf{q}^T \mathbf{D}^H \mathbf{q} / \|\mathbf{q}\|^2$  as the diffusion time,  $(\Delta - \delta/3)$ , increases. This fact follows directly from homogenization theory, because the diffusion behavior of the homogenized system is the limit, as time goes infinity, of the diffusion behavior of heterogeneous Bloch-Torrey PDE model [23]. Hence, the  $ADC_0$  of the latter approaches  $D^H$ , which is the  $ADC_0$  of the homogenized system. Nevertheless, we conducted some numerical experiments to illustrate the time convergence of  $ADC_0$  to  $D^H$ . For simplicity, we chose  $\mathbf{q}/\|\mathbf{q}\| = [0,0,1]$ .

First we show that  $ADC_0$  obtained by applying the biexponential model (eq. [8], [10]) using 12  $b$ -values between 0 and 4000  $s/mm^2$  and the cumulant expansion model (eq. [9]) using 5  $b$ -values between 0 and 500  $s/mm^2$  are quite close to each other. We computed the DMRI signal by numerically solving Bloch-Torrey equations [1]-[4] with the PGSE sequence  $\delta=2.5ms$ ,  $\Delta=10$  to 85ms (in 5ms intervals) at  $b = 0, 50, 100, 200, 500, 1000, 1500, 2000, 2500, 3000, 3500, 4000$   $s/mm^2$  in the gradient direction  $\mathbf{q}/\|\mathbf{q}\| = [0,0,1]$ . On the domain of the randomly oriented and placed cylinders and spheres (Fig 1D) with  $v^e = 0.17$  and  $D^e=D^i=3 \times 10^{-3} mm^2/s$ ,  $\kappa = 10^{-5} m/s$ , the signal attenuation at the 5 lowest  $b$ -values do not vary much with diffusion time (shown in Fig 3 for  $\Delta = 10, 20, 30, 40ms$ ), as opposed to the higher  $b$ -values, which have higher relative variations with diffusion time. We see from Fig 3 (the legend) that  $ADC_0^{poly}$  and  $ADC_0^{biexp}$  differ less than 3%. Thus, in the rest of the paper,  $ADC_0$  will be computed by a quadratic fit of 5  $b$ -values between 0 and 500  $s/mm^2$ .



In Fig 4A, we show the convergence as the diffusion time increases (from  $\Delta=10 \text{ ms}$  to  $\Delta=85 \text{ ms}$ ) of  $ADC_0$  (in the gradient direction  $[0,0,1]$ ) to the homogenized diffusion coefficient  $D^H$  (the third eigenvalue of homogenized diffusion tensor  $\mathbf{D}^H$ ) for the geometries shown in Fig 1A (cubes) and Fig 1D (random cylinders and spheres) with  $D^e=D^i=3 \times 10^{-3} \text{ mm}^2/\text{s}$ ,  $\kappa = 10^{-5} \text{ m/s}$  and  $\kappa = 5 \times 10^{-5} \text{ m/s}$ . In Fig 4B, we plotted the inverse diffusion time  $(\Delta-\delta/3)^{-1}$  on the x-axis in log scale and the absolute value of  $ADC_0/D^H-1$  on the y-axis in log scale. We see a clearly linear relationship between the log of the diffusion time and the log of the relative difference between  $ADC_0$  and  $D^H$ , suggesting the fit  $ADC_0 \approx D^p + C/(\Delta-\delta/3)^\alpha$ , where  $D^H$  is expected to be close to the extrapolated value  $D^p$  at infinite diffusion time, and  $\alpha > 0$  is the exponent of time convergence. In the legend of Fig 4B, we include the 95% confidence interval of the estimate of  $\alpha$ , which is  $[1.17, 1.18]$  for cubes at  $\kappa = 10^{-5} \text{ m/s}$ ,  $[0.98, 0.99]$  for cubes at  $\kappa = 5 \times 10^{-5} \text{ m/s}$ ,  $[0.57, 0.59]$  and  $[0.74, 0.77]$  for the cylinders and spheres at low and high permeabilities,

respectively. The range of  $\alpha$  that we obtained here is consistent with the results of [34] (for the special case of  $v^e = 0$ ). In Fig 4C, we computed the 95% confidence intervals for the fit of  $D^p$ , the extrapolated value at infinite diffusion time, using 5 values of  $\Delta = [65, 70, 75, 80, 85]$  ms. We obtained that the relative difference between  $D^H$  and the 95% interval of  $D^p$  is less than 3% for both geometries and both permeabilities (see legend of Fig 4C).

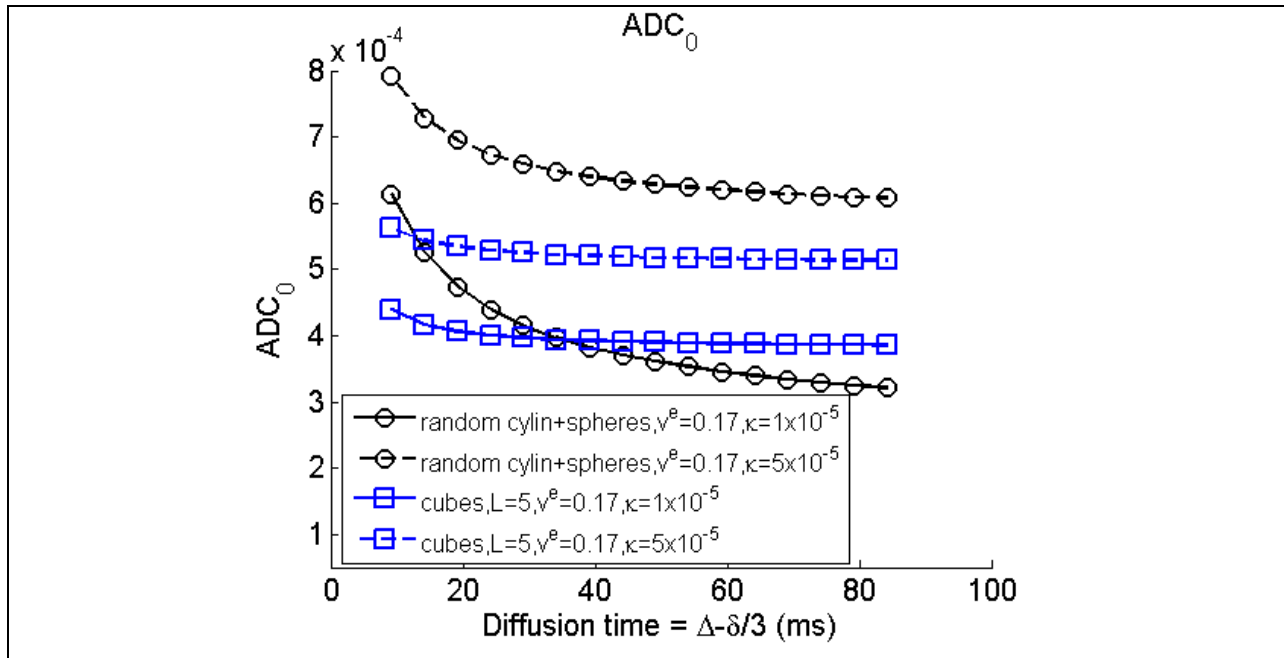


Fig 4A

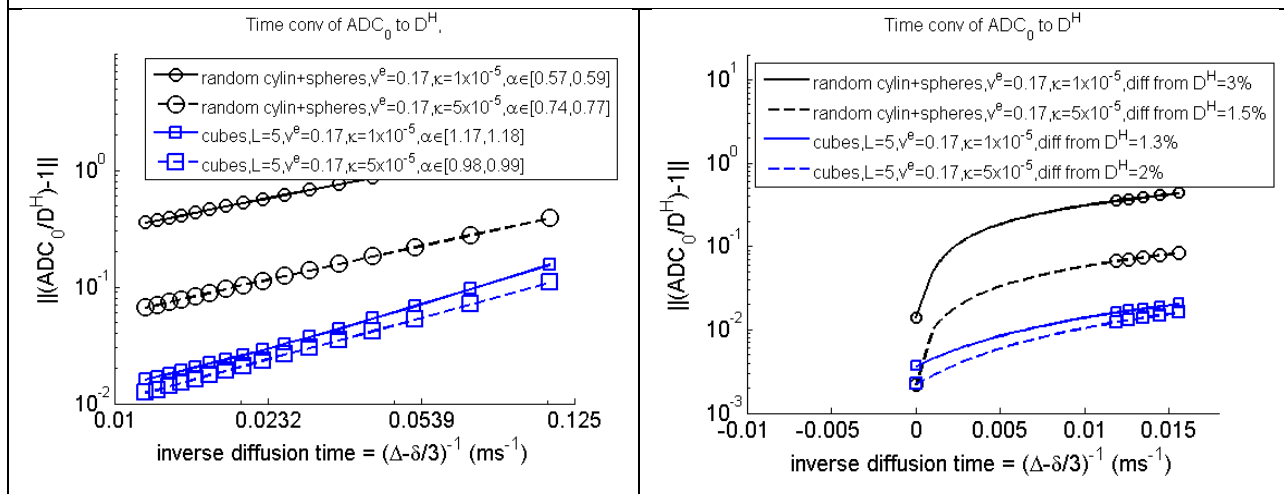


Fig 4B

Fig 4C

### 3. Relationship of $D^H$ to tissue parameters and the approximate analytical formulae.

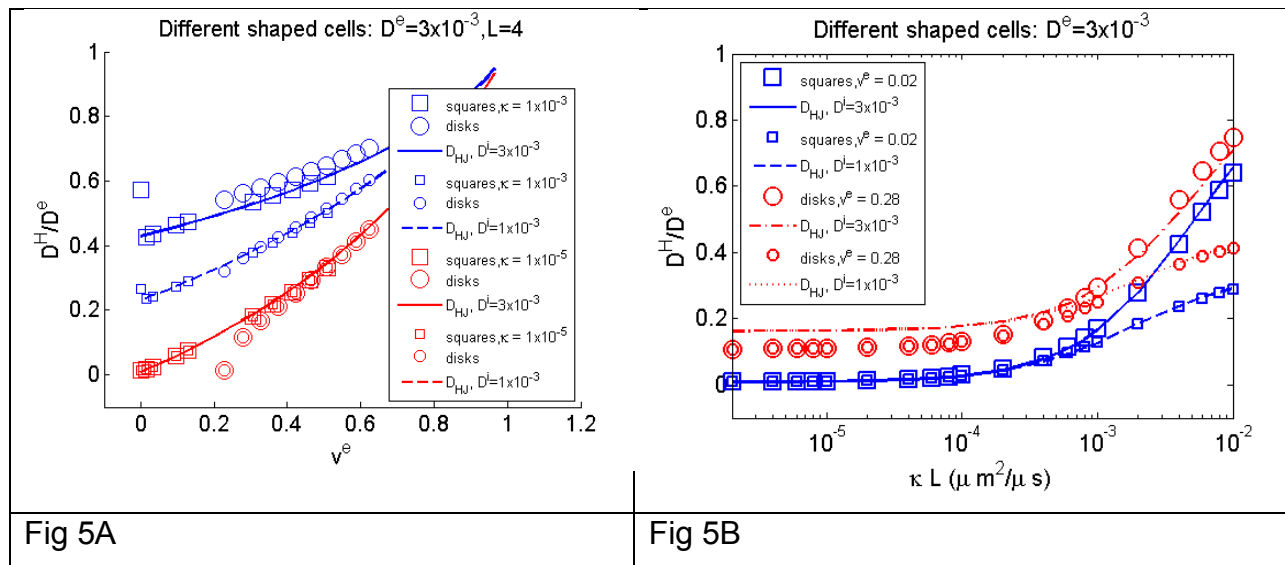
The analytical formulae  $D_{HJ}$  (2D),  $D_{TR}$  (3D) (Eq. [14]) and  $D_{LSMS}$  (3D) (Eq. [17]) are not exact and are derived as approximations of  $D^H$  for periodic spherical cells and moderate  $v^i$ . However, we now show numerically that they are also accurate for more general geometrical shapes and high  $v^i$  (low extra-cellular volume), as long as the cells are not too elongated, and if the most of the diffusion occurs in the extra-cellular space, rather than directly between neighboring cells.

In Fig 5A, we plot  $D^H$  for two-dimensional array of square cells, marked 'squares', and two-dimensional array of circular cells, marked 'disks', for  $L = 4 \mu\text{m}$ ,  $D^e = 3 \times 10^{-3} \text{mm}^2/\text{s}$ ,  $D^i = 3 \times 10^{-3} \text{mm}^2/\text{s}$  or  $D^i = 1 \times 10^{-3} \text{mm}^2/\text{s}$ , and membrane permeability  $\kappa = 10^{-5} \text{m/s}$  or  $\kappa = 10^{-5} \text{m/s}$  for a wide range of  $v^e$ . We plot the  $D^H$  normalized by the intrinsic extra-cellular diffusion coefficient  $D^e$ . We see that at low permeability, there is no difference in  $D^H$  between  $D^i = 3 \times 10^{-3} \text{mm}^2/\text{s}$  and  $D^i = 1 \times 10^{-3} \text{mm}^2/\text{s}$ . Thus, we remark that the  $D^H$  reflects mainly the extra-cellular space at low permeability. We also see that it is not possible to distinguish between circular and square shapes at low permeability. As long as there is a contiguous (unbounded in space) extra-cellular domain, the circular and square cells fall on the same curve, which varies only with  $v^e$  and not the shape of the cells. This curve is very accurately described by the analytical formula  $D_{HJ}$ . However, one can see that the curve for the circular cells behaves differently than that for the square cells as  $v^e$  approaches 0.22, i.e., when the circular cells begins to touch each other at a tangent point. Once the circular cells make contact, the extra-cellular space is cut into non-contiguous sections, and the  $D^H$  rapidly decreases to 0 as shown in Fig 5A at low permeability.

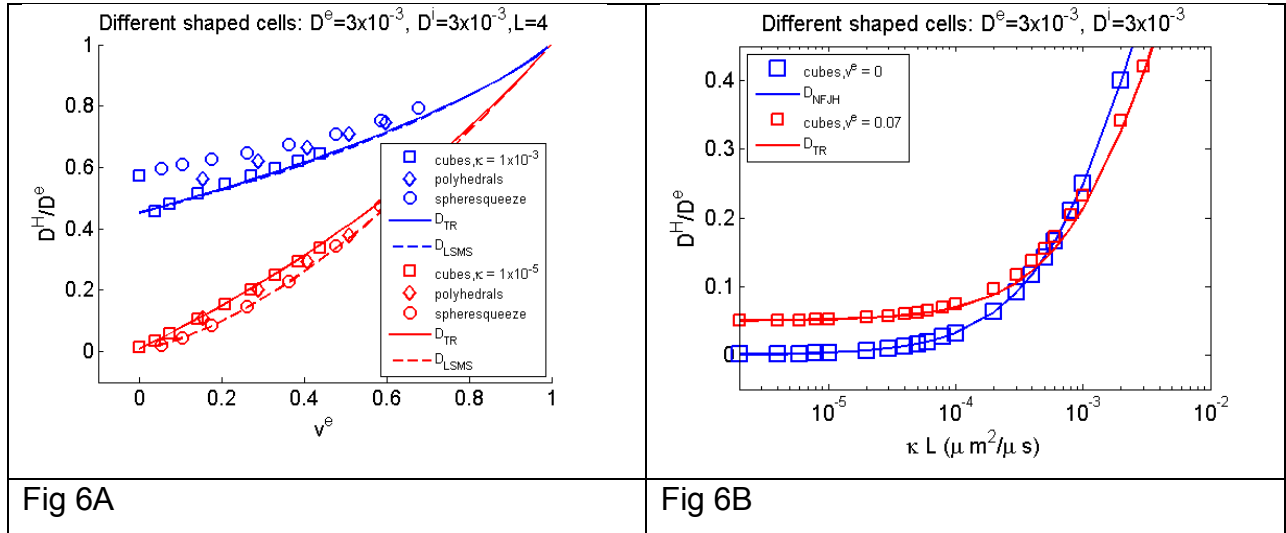
With square cells, at high permeability, we see an odd phenomenon: the  $D^H$  at  $v^e = 0$  is higher than at  $v^e = 0.2$ . This is strange because  $D^H$  is a decreasing function of  $v^e$  if we

look only at all the  $v^e$  strictly  $> 0$ . The physical explanation of why  $D^H$  at  $v^e = 0$  is higher than nearby  $v^e > 0$  for high permeability is that at higher permeability, the water molecules have an easier time going directly from cell to cell when  $v^e = 0$ , as compared to having to go through two membranes when the extra-cellular space still exists (nearby small  $v^e > 0$ ). But at lower permeability, water molecules have a hard time going directly from cell to cell, so the  $D^H$  at  $v^e = 0$  is lower than nearby  $v^e > 0$ .

In Fig 5B, we show that  $D^H$  depends only on the product  $\kappa L$ , in other words, as long as the product of  $\kappa$  and  $L$  remains constant,  $D^H$  will be constant. This fact is easy to see from the analytical formula  $D_{HJ}$ , but we also show it numerically by computing  $D^H$  for many  $\kappa = 10^{-2}, 10^{-3}, 10^{-4}, 10^{-5}, 10^{-6}$  m/s and  $L = 2, 4, 6, 8, 10$   $\mu m$  and plotting  $D^H$  as a function of  $\kappa L$ . Clearly, we see all the  $D^H$ , given a fixed  $v^e$ , fall on the same curve when plotted against the product  $\kappa L$ . And again, at low  $\kappa$ ,  $D^i = 3 \times 10^{-3} mm^2/s$  and  $D^i = 1 \times 10^{-3} mm^2/s$  cannot be distinguished. We note  $D_{HJ}$  is less accurate at high  $v^e$ . In addition, we can see that while keeping  $\kappa$  constant, changing  $L$  has a small effect on  $D^H$  unless  $\kappa$  is very large.



Now we show numerical results for three-dimensional geometries. The first example is periodic cubic cells (Fig 1A) where the distance between the cell boundaries is  $h$ , which we varied from 1% to 10% of  $L$ , the inter-cell distance. In other words, when  $h > 0$ , the cubic cells do not touch each other. Polyhedral cells (Fig 1C) also do not touch each other; the distance between the polyhedral cells is also  $h$ . The spherical cells (Fig 1B) are squeezed together: we enlarge the radius of the spheres, but we do not allow the spheres to cross each other. The squeezed spherical geometry is interesting because the cells touch their neighbors in an area that becomes larger as the cellular volume fraction increases. We can increase the cellular volume fraction of squeezed spherical cells to 100%, at which point, this geometry becomes cubic cells with no extra-cellular space. The cubic cells provide an extra-cellular space that is always at least  $h$  wide. The squeezed spherical cells provide an extra-cellular space that is pinched in the areas where the neighboring cells touch, so this extra-cellular is more tortuous.



In Fig 6A, we plot the normalized  $D^H$  of cubic, polyhedral, and squeezed spherical cells. The  $D^H$  of cubic cells can be accurately approximated by the analytical formula  $D_{TR}$  for both high and low permeability (except at  $v^e = 0$  and high permeability due to direct diffusion from cell to cell without passing through extra-cellular space, as discussed already in the two-dimensional example above). At low permeability, the  $D^H$  of the squeezed spherical cells is accurately approximated by the analytical formula  $D_{LSMS}$ .

Hence, we conclude that  $D_{TR}$  is useful when the extra-cellular space is of a uniform width (h in the case of cubic cells) and  $D_{LSMS}$  is useful when the extra-cellular space is pinched off by neighboring cells touching each other. For both, there must not be a lot of direct diffusion from cell directly to neighboring cell. At high permeability, because the effect of direct diffusion between cells, the  $D^H$  of the squeezed spheres is much higher than that given by the formula  $D_{LSMS}$ . The  $D^H$  of the polyhedral cells is close to the cubic cells, especially, at low permeability, supporting the argument again that at low permeability, the shape of the cells cannot be distinguished, only the extra-cellular volume fraction.

In Fig 6B, we show that in three dimensions also, only the product  $\kappa L$  affects  $D^H$ , not  $\kappa$  and  $L$  separately, by simulating  $\kappa = 10^{-2}, 10^{-3}, 10^{-4}, 10^{-5}, 10^{-6}$  m/s and  $L = 2, 4, 6, 8, 10$   $\mu\text{m}$  and plotting  $D^H$  against  $\kappa L$ . Only cubic cells are shown, but the other geometries also exhibit this property. We also include the computed  $D^H$  for cubic cells when  $v^e = 0$  and show that it is perfectly described by the analytical formula  $D_{NFJH}$ . It is clear at low permeability, because the diffusion is controlled via the extra-cellular space,  $v^e = 0$  results in a lower  $D^H$  than a small  $v^e > 0$ ,  $v^e = 0.07$  in this case. However, at higher permeability, because the important contribution of the direct diffusion between neighboring cells without passing through the extra-cellular space, the  $D^H$  at  $v^e = 0$  is greater than the  $D^H$  at a small  $v^e = 0.07$ . This conclusion may seem counter-intuitive, but it is clearly illustrated in Fig 6B. In addition, as in two dimensions, we can see that changing  $\kappa L$  has a very small effect on  $D^H$  unless  $\kappa L$  is very large.

## Discussion

Effects of diffusion on the MRI signal are generally described with the Bloch-Torrey PDE. This PDE can be applied to some tissue models, e.g., the presence of two or three compartments, such as the intra-cellular, extra-cellular and membrane compartments. However, for these multiple compartment models, solutions to this PDE cannot be obtained analytically.

In this paper, we conducted an analytical and numerical study of the first moment of the log of the DMRI signal in  $b$ -value at  $b=0$ , denoted  $ADC_0$ , that we obtained by fitting a quadratic polynomial to the log signal at low  $b$ -values (between 0 and  $500 \text{ s/mm}^2$ ). We showed that as the diffusion time increases,  $ADC_0$  approaches  $D^H$ , the homogenized diffusion coefficient, which we showed can be obtained by solving a set of time-independent PDEs that are easier to solve than the time-dependent Bloch-Torrey PDE. This way of computing  $D^H$  is valid for arbitrary cellular geometries.

In addition, we showed that three analytical formulae originally derived for  $D^H$  of periodic spherical cells:  $D_{HJ}$ ,  $D_{TR}$  (Eq. [14]) and  $D_{LSMS}$  (Eq. [17]), also work well for more general shapes of cells at relatively low permeability, as long as the cells are not too elongated and an average inter-cell distance can be defined.

We showed that  $D^H$  is mainly an indicator of the extra-cellular space at low permeability: decreasing the intrinsic intracellular diffusion coefficient by a factor of 3 had no impact on  $D^H$  at low permeability. Increasing the average inter-cell distance (increasing cell size at the expense of the cell density so that the total cellular volume fraction remained constant) leads to a moderate decrease in  $D^H$  only at high cell permeability. On the other hand  $D^H$  is much affected by changing in the extracellular volume fraction  $v^e$ , a much more efficient mechanism linking variations of  $D^H$  with cell size. We infer that at long diffusion times and low  $b$ -values water molecules which have remained in cells (not crossing cell membranes), do not contribute much to the signal attenuation.

From experimental point of view, the microstructure of a tissue is not known and has to be inferred by DMRI, in particular, through ADC. We have showed that if  $ADC_0$  is obtained at several 'long' diffusion times, even if they are still different from  $D^H$ , some kind of extrapolation procedure is expected to allow one to get  $D^H$  from those  $ADC_0$  values. Once  $D^H$  has been obtained in this way, we hope to be able to use the relationship of  $D^H$  to the tissue parameters, or the analytical approximations to  $D^H$  that we studied in this paper, to draw certain conclusions about the tissue sample, keeping



in mind of course, that these conclusions will mainly concern the extra-cellular space. This is a possible direction of future work.

In practice, in *in vivo* imaging, the signal attenuation at very low  $b$  values would be very noisy as the level of signal attenuation would be small and the effects of blood microcirculation (Intra-voxel Incoherent Motion or IVIM, REF DLB 1988) would interfere with the  $ADC_0$  estimation. Hence, the slope at  $b = 0$  should be extrapolated from the log of the whole signal curve obtained from a large range of  $b$ -values and fitted either as a polynomial function or a bi-exponential function, and then the slope of this function should be computed analytically at  $b = 0$  to give  $ADC_0$ .

The two most biologically relevant geometries of tissues that we simulated in this paper are the randomly oriented and placed cylindrical and spherical cells (Fig 1D) for modeling cerebral grey matter and the squeezed spherical cells (Fig 1B) for modeling tumor cells.

In the brain cortex, cell shapes are very complex, they may be “star” like, with neural bodies extended by long axons and dendrites. Indeed, in the brain cortex neuronal cell bodies measure approximately 1 to 10  $\mu\text{m}$ , occupying 12% of the cortex volume, while the rest is occupied by the neuropile (34% by axons, 35% by dendrites, measuring respectively 0.5 and 0.9  $\mu\text{m}$  in average), 14% by spines and 6% by the extracellular space which is of the order of 10–30 nm (REF). A lower-limit of around 0.5  $\mu\text{m}$  for intracellular dimensions has been estimated in the synaptic neuropile, which contains the highest density of cellular membranes in gray matter (REF). Furthermore, many subcellular structures, such as mitochondria, vesicles, nuclear membranes also represent obstacles to diffusion. In short, about 90% of cellular elements in the brain cortex are smaller than 1 $\mu\text{m}$ . Hence, an improvement of the geometry in Fig 1D (randomly oriented and placed cylinders and spheres) would be necessary to model realistic brain tissue. Such improvements are feasible and present another direction of future work.

In summary,  $ADC_0$ , the first moment, at low  $b$ -value, of the log of the DMRI signal attenuation at long diffusion time is mainly a marker of the extracellular space. It can provide information on tissues, as most changes in tissue structure (cell size, cell density) would usually impact the extracellular space fractional volume, but only from an indirect way, i.e., a “negative”, connected imprint of the cellular network. Indeed, the long diffusion time  $ADC_0$  will miss tissue structure events involving solely the intracellular space. Clearly, to complete the picture and get information on the intracellular space as well, signal from high  $b$ -values (above 3000 or 4000  $s/mm^2$ ) must be included in the diffusion models. Diffusion studies performed at short diffusion times, when intra-cellular diffusion is not yet quenched, on preclinical scanners equipped with high performance gradient system, would also provide highly valuable information on tissue structure (REF NADYA).

# Appendix

## ***Derivation of the steady-state two-compartment model formula***

In the usual formulation of the multiple compartments homogenization problem, the permeability across interfaces is assumed to be infinite, i.e., the concentration is continuous across the interface. In our problem, the interface permeability  $\kappa$  is finite and there is a discontinuity in the concentration on the interface.

We derive the time-independent formulation for the two-compartment homogenization problem (shown in Eq. [13]) by introducing an artificial third compartment: an interface compartment consisting of a layer of thickness  $h$  lying on the interface between  $\Omega^e$  and  $\Omega^i$ . We will label the original interface between  $\Omega^e$  and  $\Omega^i$  by  $\Gamma$  and we will label the outer boundary of the artificial interface layer by  $\Gamma^{e,h} \equiv \Gamma + \frac{h}{2}\mathbf{n}$  and the inner boundary of the interface layer by  $\Gamma^{i,h} \equiv \Gamma - \frac{h}{2}\mathbf{n}$ . We shall label the artificial interface layer  $\Omega^{i,h}$  and the associated inter-cellular compartment  $\Omega^{j,h}$  and the associated extra-cellular compartment  $\Omega^{e,h}$ .

We will start with the standard formulation where the concentration is continuous at the interfaces between the three compartments, i.e., the permeability between  $\Omega^{e,h}$  and  $\Omega^{j,h}$  (on  $\Gamma^{e,h}$ ) and between  $\Omega^{j,h}$  and  $\Omega^{i,h}$  (on  $\Gamma^{i,h}$ ) is assumed to be infinite. To mimic the effect of the finite permeability  $\kappa$  between  $\Omega^e$  and  $\Omega^i$  we impose an intrinsic diffusion coefficient  $D^{l,h}$  in the layer that depends on  $h$  in the following way:

$$D^{l,h} \equiv \kappa h. \quad [19]$$

To first order, this relationship will ensure that the permeability condition between  $\Omega^e$  and  $\Omega^i$  (Eq. [4]) is satisfied.

The standard formulation of the three-compartment homogenization PDE is the following for each coordinate direction  $m$  [23]:

$$\begin{aligned}
\nabla \cdot (D^j \nabla u_m^{j,h}(\mathbf{x})) &= 0, & \mathbf{x} \in \Omega^{j,h}, & \quad j = i, e, \\
\nabla \cdot (D^{l,h} \nabla u_m^{l,h}(\mathbf{x})) &= 0, & \mathbf{x} \in \Omega^{l,h}, & \\
D^j \nabla u_m^{j,h}(\mathbf{x}) \cdot \mathbf{n}(\mathbf{x}) &= D^{l,h} \nabla u_m^{l,h}(\mathbf{x}) \cdot \mathbf{n}(\mathbf{x}), & \mathbf{x} \in \Gamma^{j,h}, & \quad j = i, e, \\
u_m^{j,h}(\mathbf{x}) - u_m^{l,h}(\mathbf{x}) &= 0, & \mathbf{x} \in \Gamma^{j,h}, & \quad j = i, e, \\
u_m^{j,h}(\mathbf{x} + L_m \mathbf{e}_m) &= u_m^{j,h}(\mathbf{x}) + L_m, & \mathbf{x}, \mathbf{x} + L_m \mathbf{e}_m \in \partial C, & \\
u_m^{j,h}(\mathbf{x} + L_n \mathbf{e}_n) &= u_m^{j,h}(\mathbf{x}), & \mathbf{x}, \mathbf{x} + L_n \mathbf{e}_n \in \partial C, & \quad n \neq m.
\end{aligned} \tag{20}$$

We will now derive the time-independent homogenized PDEs in the limit as  $h$  goes to 0, which is given in Eq. [13]. In Eq. [20] it is not difficult to see the limit as  $h$  goes 0 of the first and the last two equations will become the first and the last two relations of Eq(13). We need only to derive equations 2 and 3 in Eq. [13].

From the third equation in Eq. [20] and the divergence theorem, we infer that  $D^{l,h} \nabla u_m^{l,h} \cdot \mathbf{n}$  is almost constant along the width of the thin layer  $\Omega^{l,h}$ , i.e.,

$$(D^{l,h} \nabla u_m^{l,h} \cdot \mathbf{n})(\mathbf{x}) \approx (D^{l,h} \nabla u_m^{l,h} \cdot \mathbf{n})\left(\mathbf{x} \pm \frac{\xi h}{2} \mathbf{n}\right), \quad 0 \leq \xi \leq 1, \mathbf{x} \in \Gamma.$$

The above approximation holds up to  $O(\delta)$  terms. Taking  $\xi = 1$ , one gets, from the third equation of Eq. [20],

$$(D^{l,h} \nabla u_m^{l,h} \cdot \mathbf{n})(\mathbf{x}) \approx (D^{l,h} \nabla u_m^{l,h} \cdot \mathbf{n})\left(\mathbf{x} + \frac{h}{2} \mathbf{n}\right) = (D^e \nabla u_m^{e,h} \cdot \mathbf{n})\left(\mathbf{y} + \frac{h}{2} \mathbf{n}\right),$$

and

$$(D^{l,h} \nabla u_m^{l,h} \cdot \mathbf{n})(\mathbf{x}) \approx (D^{l,h} \nabla u_m^{l,h} \cdot \mathbf{n})\left(\mathbf{x} - \frac{h}{2} \mathbf{n}\right) = (D^i \nabla u_m^{i,h} \cdot \mathbf{n})\left(\mathbf{y} - \frac{h}{2} \mathbf{n}\right).$$

Therefore

$$(D^e \nabla u_m^{e,h} \cdot \mathbf{n})\left(\mathbf{y} + \frac{h}{2} \mathbf{n}\right) = (D^i \nabla u_m^{i,h} \cdot \mathbf{n})\left(\mathbf{y} - \frac{h}{2} \mathbf{n}\right),$$

which is what we need to obtain the second equation of Eq. [13].

Next, using a Taylor expansion, for  $\mathbf{y} \in \Gamma$ ,

$$u_m^{l,h}\left(\mathbf{y} + \frac{h}{2} \mathbf{n}\right) - u_m^{l,h}\left(\mathbf{y} - \frac{h}{2} \mathbf{n}\right) \approx h(\nabla u_m^{l,h} \cdot \mathbf{n})(\mathbf{y}) = \frac{1}{\kappa} (D^{l,h} \nabla u_m^{l,h} \cdot \mathbf{n})(\mathbf{y}).$$

We then obtain, using the third and fourth equations in Eq. [20],

$$u_m^{e,h}\left(\mathbf{y} + \frac{h}{2} \mathbf{n}\right) - u_m^{i,h}\left(\mathbf{y} - \frac{h}{2} \mathbf{n}\right) \approx \frac{1}{\kappa} (D^{i,h} \nabla u_m^{i,h} \cdot \mathbf{n})\left(\mathbf{y} - \frac{h}{2} \mathbf{n}\right), \quad \mathbf{y} \in \Gamma.$$

Taking the limit  $h = 0$ , we obtain of third equation of Eq. [13].

## References

- [1] D. Le Bihan and H. Johansen-Berg, "Diffusion mri at 25: Exploring brain tissue structure and function," *NeuroImage*, no. 0, pp. –.
- [2] S. Warach, D. Chien, W. Li, M. Ronthal, and R. R. Edelman, "Fast magnetic resonance diffusion-weighted imaging of acute human stroke," *Neurology*, vol. 42, no. 9, pp. 1717–, 1992.
- [3] Y. Hasegawa, M. Fisher, L. L. Latour, B. J. Dardzinski, and C. H. Sotak, "Mri diffusion mapping of reversible and irreversible ischemic injury in focal brain ischemia," *Neurology*, vol. 44, no. 8, p. 1484, 1994.
- [4] T. Sugahara, Y. Korogi, M. Kochi, I. Ikushima, Y. Shigematu, T. Hirai, T. Okuda, L. Liang, Y. Ge, Y. Komohara, Y. Ushio, and M. Takahashi, "Usefulness of diffusion-weighted mri with echo-planar technique in the evaluation of cellularity in gliomas," *J. Magn. Reson. Imaging*, vol. 9, no. 1, pp. 53–60, 1999.
- [5] D. Schnapauff, M. Zeile, M. B. Niederhagen, B. Fleige, P.-U. Tunn, B. Hamm, and O. Dudeck, "Diffusion-weighted echo-planar magnetic resonance imaging for the assessment of tumor cellularity in patients with soft-tissue sarcomas," *J. Magn. Reson. Imaging*, vol. 29, no. 6, pp. 1355–1359, 2009.
- [6] Y. Tsushima, A. Takahashi-Taketomi, and K. Endo, "Magnetic resonance (mr) differential diagnosis of breast tumors using apparent diffusion coefficient (adc) on 1.5-t," *J. Magn. Reson. Imaging*, vol. 30, no. 2, pp. 249–255, 2009.
- [7] D. LeBihan, S.-i. Urayama, T. Aso, T. Hanakawa, and H. Fukuyama, "Direct and fast detection of neuronal activation in the human brain with diffusion mri," *PNAS*, vol. 103, no. 21, pp. 8263–8268, 2006.
- [8] D. L. Buckley, J. D. Bui, M. I. Phillips, and S. J. Blackband, "Mri measurement of cell volume fraction in the perfused rat hippocampal slice," *Magn. Reson. Med.*, vol. 42, no. 3, pp. 603–607, 1999.
- [9] J. Flint, B. Hansen, P. Vestergaard-Poulsen, and S. J. Blackband, "Diffusion weighted magnetic resonance imaging of neuronal activity in the hippocampal slice model," *NeuroImage*, vol. 46, pp. 411–418, June 2009.
- [10] R. Andrew and B. Macvicar, "Imaging cell volume changes and neuronal excitation in the hippocampal slice," *Neuroscience*, vol. 62, pp. 371–383, Sept. 1994.
- [11] D. LeBihan, "The 'wet mind': water and functional neuroimaging.," *Physics in medicine and biology*, vol. 52, pp. –, Apr. 2007.
- [12] I. TASAKI *The Japanese Journal of Physiology*, vol. 49, no. 2, pp. 125–138, 1999.
- [13] D. Grebenkov, "Nmr survey of reflected brownian motion," *Reviews of Modern Physics*, vol. 79, no. 3, pp. 1077–1137, 2007.
- [14] D. S. Grebenkov, "Laplacian eigenfunctions in nmr. ii. theoretical advances," *Concepts Magn. Reson.*, vol. 34A, no. 5, pp. 264–296, 2009.

- [15] S. N. Hwang, C.-L. Chin, F. W. Wehrli, and D. B. Hackney, "An image-based finite difference model for simulating restricted diffusion," *Magnetic Resonance in Medicine*, vol. 50, no. 2, pp. 373–382, 2003.
- [16] J. Xu, M. Does, and J. Gore, "Numerical study of water diffusion in biological tissues using an improved finite difference method.," *Physics in medicine and biology*, vol. 52, pp. –, Apr. 2007.
- [17] K. D. Harkins, J.-P. Galons, T. W. Secomb, and T. P. Trouard, "Assessment of the effects of cellular tissue properties on adc measurements by numerical simulation of water diffusion," *Magn. Reson. Med.*, vol. 62, no. 6, pp. 1414–1422, 2009.
- [18] M. Hall and D. Alexander, "Convergence and parameter choice for monte-carlo simulations of diffusion mri," *Medical Imaging, IEEE Transactions on*, vol. 28, pp. 1354–1364, Sept. 2009.
- [19] G. T. Balls and L. R. Frank, "A simulation environment for diffusion weighted mr experiments in complex media," *Magn. Reson. Med.*, vol. 62, no. 3, pp. 771–778, 2009.
- [20] K. D. Harkins, J.-P. Galons, J. L. Divijak, and T. P. Trouard, "Changes in intracellular water diffusion and energetic metabolism in response to ischemia in perfused c6 rat glioma cells," *Magn. Reson. Med.*, vol. 66, no. 3, pp. 859–867, 2011.
- [21] H. Torrey, "Bloch equations with diffusion terms," *Physical Review Online Archive (Prola)*, vol. 104, no. 3, pp. 563–565, 1956.
- [22] D. S. Grebenkov, "Pulsed-gradient spin-echo monitoring of restricted diffusion in multilayered structures," *Journal of Magnetic Resonance*, vol. 205, pp. 181–195, Aug. 2010.
- [23] A. Bensoussan, J.-L. Lions, and G. Papanicolaou, *Asymptotic analysis for periodic structures*, vol. 5 of *Studies in Mathematics and its Applications*. Amsterdam: North-Holland Publishing Co., 1978.
- [24] D. Le Bihan, E. Breton, D. Lallemand, P. Grenier, E. Cabanis, and M. Laval-Jeantet, "Mr imaging of intravoxel incoherent motions: application to diffusion and perfusion in neurologic disorders.," *Radiology*, vol. 161, no. 2, pp. 401–407, 1986.
- [25] E. O. Stejskal and J. E. Tanner, "Spin diffusion measurements: Spin echoes in the presence of a time-dependent field gradient," *The Journal of Chemical Physics*, vol. 42, no. 1, pp. 288–292, 1965.
- [26] T. Niendorf, R. M. Dijkhuizen, D. G. Norris, M. van Lookeren Campagne, and K. Nicolay, "Biexponential diffusion attenuation in various states of brain tissue: Implications for diffusion-weighted imaging," *Magn. Reson. Med.*, vol. 36, no. 6, pp. 847–857, 1996.
- [27] J. Karger, H. Pfeifer, and W. Heinik, "Principles and application of self-diffusion measurements by nuclear magnetic resonance," *Advances in magnetic resonance*, vol. 12, pp. 1–89, 1988.
- [28] E. X. Wu and M. M. Cheung, "Mr diffusion kurtosis imaging for neural tissue characterization," *NMR Biomed.*, vol. 23, no. 7, pp. 836–848, 2010.
- [29] D. A. Yablonskiy and A. L. Sukstanskii, "Theoretical models of the diffusion weighted mr signal," *NMR Biomed.*, vol. 23, no. 7, pp. 661–681, 2010.

- [30] H. Cheng and S. Torquato, "Effective conductivity of periodic arrays of spheres with interfacial resistance," *Proceedings: Mathematical, Physical and Engineering Sciences*, vol. 453, pp. 145–161, Jan. 1997.
- [31] D. Hasselman and L. F. Johnson, "Effective thermal conductivity of composites with interfacial thermal barrier resistance," *Journal of Composite Materials*, vol. 21, pp. 508–515, June 1987.
- [32] S. Torquato and M. D. Rintoul, "Effect of the interface on the properties of composite media," *Phys. Rev. Lett.*, vol. 75, pp. 4067–, Nov. 1995.
- [33] L. L. Latour, K. Svoboda, P. P. Mitra, and C. H. Sotak, "Time-dependent diffusion of water in a biological model system.," *Proceedings of the National Academy of Sciences*, vol. 91, no. 4, pp. 1229–1233, 1994.
- [34] D. S. Novikov, E. Fieremans, J. H. Jensen, and J. A. Helpert, "Random walks with barriers," *Nat Phys*, vol. 7, pp. 508–514, June 2011.
- [35] J. H. Jensen and J. A. Helpert, "Progress in diffusion-weighted imaging: concepts, techniques and applications to the central nervous system," *NMR Biomed.*, vol. 23, no. 7, pp. 659–660, 2010.